

Reorientation of magnetic stripe domains by mid-infrared pulsesMaxime Gidding ^{*}, Carl S. Davies , and Andrei Kirilyuk *FELIX Laboratory, Radboud University, Toernooiveld 7, 6525 ED Nijmegen, The Netherlands*

(Received 8 November 2023; revised 12 January 2024; accepted 30 January 2024; published 23 February 2024)

Several studies have explored how phononic switching of magnetization can be achieved in doped films of yttrium iron garnet (YIG) with an initially homogeneous magnetic state. In this paper, we investigate how this mechanism operates in high-purity YIG films with a nonuniform stripe domain structure. We demonstrate that a mid-infrared pulse causes the stripe domains to rotate and form a distinctive nonuniform pattern that ultimately follows the sample's easy axes. Irradiation with subsequent pulses progressively displaces the reoriented domains, thus extending the total affected area. Micromagnetic simulations, modeling the excitation as a strain pulse, provide a conceptual understanding of the observed magnetization pattern. Our observations thus extend the mechanism of phononic switching of magnetization—which manifests as stripe reorientation in the stripe domain structure—which was previously observed only in homogeneous magnetic textures.

DOI: [10.1103/PhysRevB.109.L060408](https://doi.org/10.1103/PhysRevB.109.L060408)

Introduction. Magnetism in general and its control at the microscopic level and ultrashort times in particular, continue to be at the forefront of technological advancements, with applications ranging from data storage [1,2] and sensors [3] to medical imaging [4,5] and cancer treatment [5]. The ability to manipulate magnetic states through various means, such as electric fields, temperature, and light, has opened up new avenues for fundamental research into magnetic materials [2,6].

Among the various methods of controlling magnetic states at ultrashort timescales, all-optical magnetization reversal processes have emerged as a promising research area with a strong application potential. These processes consist of a group of related—but fundamentally different—reversal mechanisms, such as optical modification of the magnetocrystalline anisotropy [7], ultrafast demagnetization in certain ferrimagnets [8–11], or helicity-dependent switching in ferromagnetic films with large spin-orbit coupling [12]. Moreover, it has recently been demonstrated that the excitation of dielectric samples at the frequencies of optical phonons can lead to the magnetization reversal characterized by peculiar domain patterns [13]. There are indications that the latter mechanism can be truly universal, as shown by similar experiments irradiating antiferromagnets [14,15] and even ferroelectrics [16] with mid- to far-infrared optical pulses. However, the exact microscopic features of this phononic mechanism are far from being fully understood, likely involving complex nonlinear interactions between phonon modes [17,18]. Moreover, the resulting nonuniform spatiotemporal dynamics of the magnetoelastic system is very complex [19].

Thus far, all studies of phononic switching of magnetization were carried out on samples in a single domain state [13,19], with a single exception of the antiferromagnetic NiO [14], where the control of the initial domain state was severely limited. A question thus emerges as to whether similar phonon-driven effects can also be observed when

starting from a multidomain magnetic state. And if so, can the modification of the domain patterns serve as a fingerprint of the excited crystallographic deformation, thus providing the necessary insights into the underlying switching mechanism?

In this paper, we examine the phononic switching of magnetization in a highly pure crystal of yttrium iron garnet (YIG) with a domain structure consisting of parallel stripes. We find that the application of infrared pulses at the frequency of optical phonons causes a reorientation of the domain pattern, nonuniformly aligning the stripe domains with one of the sample's threefold axes of magnetocrystalline anisotropy. Intriguingly, the application of multiple pulses results in these reoriented stripe domains being pushed outwards, with the direction of the displacement depending on the initial orientation of the domain stripes. Micromagnetic calculations can reproduce this behavior, providing a qualitative understanding of the excitation mechanism.

Sample and methods. The sample used in all experiments is a single-crystal 5- μm -thick undoped film of YIG grown via liquid phase epitaxy on a (111)-oriented gadolinium gallium garnet (GGG) substrate [20]. Magnetic stripe domains of width 3.5 μm , featuring magnetization that predominantly points out of plane, emerge in this sample due to the competition between the film's shape anisotropy and its stress-induced uniaxial magnetocrystalline anisotropy (MCA) [21]. Such stripe domains can be easily visualized using magneto-optical microscopy. In addition, as shown in the inset of Fig. 1, the sample possesses in its plane a weak triaxial MCA [22], which causes the striped magnetic domains to orient along one of three directions in its fully relaxed ground state. However, the orientation of these stripes can easily be manipulated in any in-plane direction through the application of in-plane magnetic fields, as the triaxial MCA is too weak to overcome the dipolar field. This offers significant control over the directionality of the magnetic domain structure.

All experiments were performed at the free-electron laser facility FELIX in the Netherlands. This light source delivers bursts (“macropulses”) of transform-limited optical

^{*}maxime.gidding@ru.nl

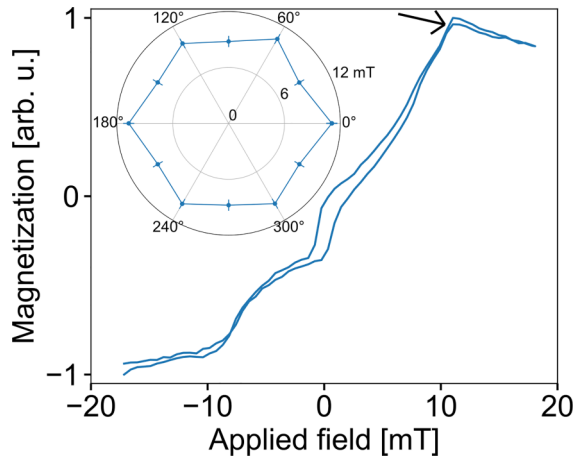


FIG. 1. Magnetic hysteresis loop of the YIG sample, obtained by applying an external magnetic field along the horizontal axis (0°) and measuring the in-plane component of magnetization via the magneto-optical Faraday effect. Inset: The measured coercive field obtained with varying in-plane orientations of the applied magnetic field. The coercive field is defined by the point at which magnetic saturation is observed, as indicated by the arrow in the main panel.

pulses with a central wavelength tuneable between 3 and $1500\ \mu\text{m}$. These $10\text{-}\mu\text{s}$ -long macropulses, coming at a rate of $10\ \text{Hz}$, enclose the picosecond-long micropulses coming at a rate of $25\ \text{MHz}$ [23]. Each burst therefore contains approximately 200 micropulses as illustrated schematically in the Supplemental Material [24]. In our experiments, we further use a fast mechanical shutter to select single macropulses. The latter are focused onto the YIG film at normal incidence using an off-axis parabolic mirror. The excitation wavelength $\lambda = 12\ \mu\text{m}$ was selected to provide an efficient modification of the domain structure by FELIX pulses, and was approximately in agreement with the spectra measured on other garnets [13,19]. The changes of the magnetic domain structure were visualized using magneto-optical Faraday microscopy at normal incidence, thus resolving the out-of-plane component of magnetization, while the orientation of the stripe domains allows us to infer the orientation of the in-plane component of magnetization.

Micromagnetic calculations were performed using the MUMAX3 package [25]. In order to allow for the inclusion of the exchange interaction in the calculations, micromagnetic cells of size $9.77 \times 9.77 \times 500\ \text{nm}^3$ were used to discretize the total sample volume $10 \times 10 \times 0.5\ \mu\text{m}^3$. The exchange constant was set to $3.7\ \text{pJm}^{-1}$ [26] and the saturation magnetization to $140\ \text{kAm}^{-1}$ [27]. It is well known that the magnetic properties of garnet films can be significantly modified by their stoichiometry [28,29], but the high purity of our yttrium-iron-garnet sample justifies our use of standard magnetic parameters [30]. The dipolar interaction was neglected. An in-plane triaxial MCA was included by providing the appropriate effective field and energy density terms, with anisotropy constant $K = 750\ \text{Jm}^3$ and the three easy axes at 120° angles relative to one another. Since we are primarily interested in the final state of the magnetization, we substantially increased the Gilbert damping constant α to 2.5 in order to speed up the micromagnetic calculations.

Unfortunately, the realistic simulation of magnetic stripe domains in extended systems is computationally unfeasible. On the one hand, inclusion of the exchange interaction limits the maximum cell size to $\approx 10\ \text{nm}$, which leads to a computer resource-limited upper bound in simulated sample dimensions on the order of $1\ \mu\text{m}^3$. On the other hand, the width of magnetic stripe domains is governed by the ratio between the MCA and the shape anisotropy [21], meaning that in order to shrink the the stripe domains to fit within the $1\ \mu\text{m}^3$ sample volume, the MCA or shape anisotropy would need to be substantially modified. Doing so would then call into question the applicability of the results. We therefore limit ourselves to considering, within the simulations, the in-plane orientation of magnetization.

In order to mimic the strain introduced by the infrared pump pulse, a strain pulse was modeled as a transient modification to the strain tensor ϵ [13,31]. Since the magnetization is compelled to stay within the sample plane, we neglect out-of-plane components. The magnetoelastic energy associated with the strain is thus defined as

$$E_{me} = B_1 (\epsilon_{xx} m_x^2 + \epsilon_{yy} m_y^2) + 2B_2 \epsilon_{xy} m_x m_y, \quad (1)$$

where ϵ_{xx} , ϵ_{xy} , ϵ_{yy} are the strain tensor components, m_x and m_y the magnetization vector components, and B_1 and B_2 are the magnetoelastic coupling constants. We set the ratio between constants B_1 and B_2 to 1:2, consistent with previous measurements of these values [32]. The Gaussian standard deviation of the strain pulse was set to $0.333\ \mu\text{m}$, which is equivalent to a full width at half maximum (FWHM) of $0.784\ \mu\text{m}$, and the full duration at half maximum τ was set to $1\ \text{ps}$. More details on the simulation of the strain pulse, along with explicit forms for the strain tensor components, can be found in the Supplemental Material [24].

Results. We start our experiments by temporarily applying a small magnetic field along the horizontal direction to similarly align the striped domain pattern across the x axis [Fig. 2(a)]. After exposing the sample to a single IR macropulse with a full width at half maximum of $13\ \mu\text{m}$, we observe that a significant portion of the magnetic stripe domains have rotated instantaneously, within the millisecond timescale afforded by our probing setup. Despite our use of an IR pulse with a symmetric Gaussian spatial profile, the spatial distribution of reoriented stripe domains is asymmetric, strongly elongated along the horizontal axis with a ratio of approximately 5:1 [top panel of Fig. 2(b)]. Moreover, upon close examination [bottom panel of Fig. 2(b)], the rotation of the stripe domains is not continuously varying but is rather aligned about a central axis that is approximately $\pm 60^\circ$ clockwise or anticlockwise relative to the x axis. As noted, this reorientation occurs across a timescale far shorter than that we can experimentally resolve, and furthermore is entirely stable in the absence of external magnetic fields.

Further irradiation of the sample with IR macropulses leads to a general expansion in the size of the affected magnetic area [top panel of Fig. 2(c)] and further reorientation of the magnetic stripes [bottom panel of Fig. 2(c)]. The affected area of magnetic domains continues to grow as the sample is exposed to more macropulses, although this expansion tends towards saturation as shown in Fig. 2(d). Finally, we find that a rotation of the initial magnetic stripe domains causes

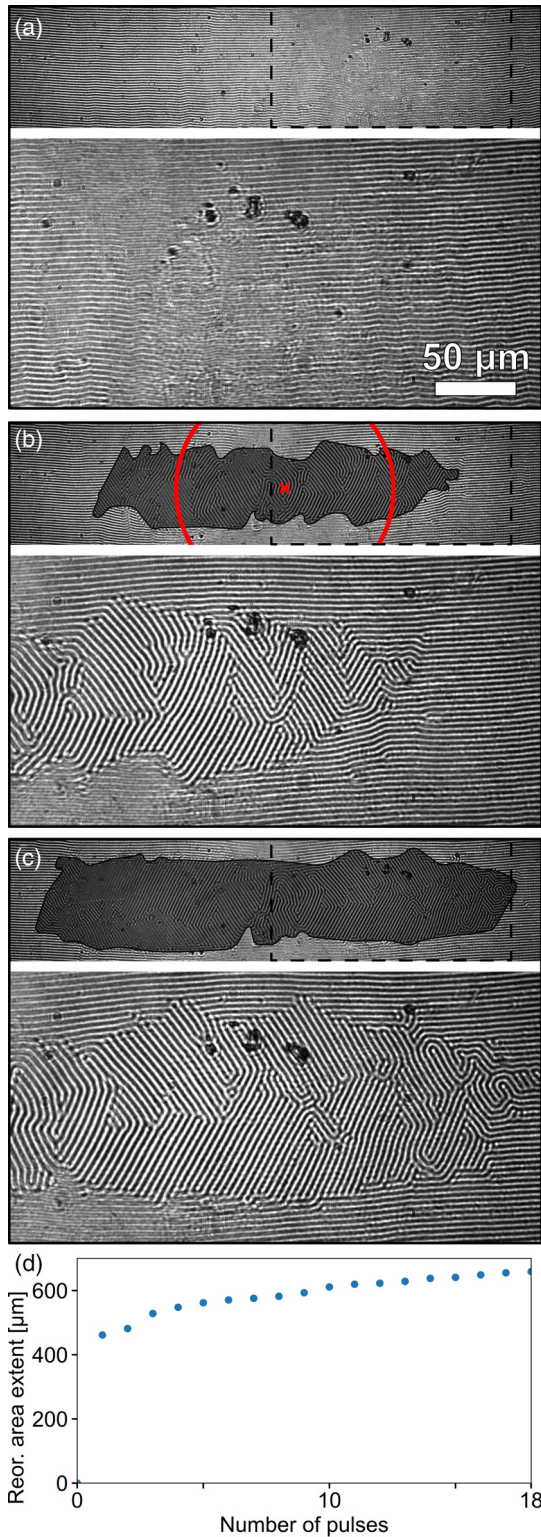


FIG. 2. (a) The domain wall orientation before application of the laser pulse. The dotted line in the top panel shows the outline of the magnified region shown in the bottom panel. (b) Full (top panel) and magnified (bottom panel) image of the domain wall reorientation after one pulse. The red outline in the top panel shows the full width at half maximum of the pump pulse. (c) Full (top panel) and magnified (bottom panel) image of the domain wall reorientation after ten pulses. (d) The horizontal extent of the reoriented area as a function of the total number of pulses.

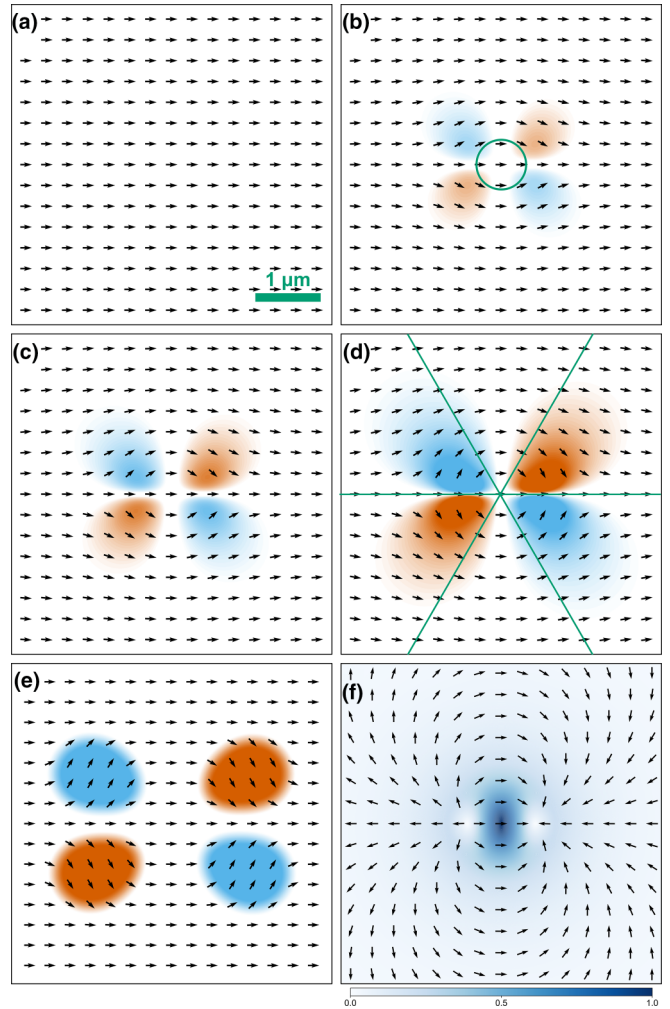


FIG. 3. Snapshots of the simulated magnetization dynamics induced by a 1-ps-long pulsed excitation, taken (a) far before the arrival of the pulse, (b), (c) 170 fs apart during the arrival of the pulse, and (d) 560 fs after the arrival of the pulse. The green circle in (b) shows the FWHM of the pump pulse, and the green lines in (d) mark the three easy axes of the triaxial magnetocrystalline anisotropy. (e) The final relaxed domain reorientation after the application of three strain pulses. (f) The distribution of the magnetoelastic field during the arrival of the pulse peak.

the overall elongated area of affected magnetization to rotate accordingly (see Supplemental Material [24]).

We proceed to perform complementary micromagnetic simulations. As discussed in the Methods section, we model a system featuring triaxial magnetocrystalline anisotropy [22], with the magnetization initially uniformly oriented along the horizontal axis. A single pulse mimicking the effect of the IR pulse is applied at the center of the simulated sample. In Figs. 3(a)–3(d), we present time-resolved snapshots of the ensuing magnetization dynamics. Upon arrival of the pulsed excitation, the magnetization immediately undergoes spatially varying rotation about the diagonals of the sample. In addition, the reoriented quadrants of magnetization grow in size. We note that as the length scale of the simulation had to be reduced compared to experiment, as discussed in the Methods section, we also reduce the energy introduced by the strain

pulses accordingly. This in turn likely leads to the reduced timescales of the simulation, compared to the experiment. The magnetization eventually settles to being aligned parallel to one of the three anisotropy axes characteristic of the modeled system.

Aiming to check how closely the micromagnetic simulation follows the experimental measurements, we expose the reoriented magnetization domains to a further train of pulses. In general, we observe that the switched quadrants grow in size after the exposure to each pulse [Fig. 3(e)], completely saturating the simulated sample after the application of eight pulses. Moreover, close examination of the magnetic domain patterns reveal that the quadrants are not symmetric about the center of the irradiated spot. Instead, the domain pattern is elongated along the horizontal axis, with an aspect ratio of about 1.4.

Discussion. Our measurements demonstrate that the stripe domains characteristic of YIG in its ground magnetic state can be reoriented by an IR pulse. Already in the images of Fig. 2, it is apparent that certain orientations of the modified stripe domains dominate. To therefore better quantify this reorientation, we calculate two-dimensional Fourier transforms of the magneto-optical images, as presented in Fig. 4. The initial uniform orientation of the stripe domains leads to a set of maxima along the y axis [Fig. 4(a)] with periodicity corresponding to the width of the domains. Upon exposure to the IR pulse, the amplitude in reciprocal space is transformed to a set of nodes corresponding to a hexagonal pattern [Fig. 4(b)]. Further exposure to IR pulses leads to a strengthening of the hexagonal pattern [Fig. 4(c)]. Figure 4(d) shows the thresholded (threshold value 10^{-2}) Fourier transform of the horizontal initial state after ten pulses, clearly showing the reorientation of the domain stripes. The overlaid hexagon has a circumscribed radius of $0.288 \mu\text{m}^{-1}$, equivalent to the stripe periodicity in the original configurations ($3.5 \mu\text{m}$), showing that the periodicity of the stripe domains is unaffected. The images used to generate Fig. 4 can be found in the Supplemental Material [24].

Figure 4 shows that the stabilized reorientation of the domain stripes occurs, in Fourier space, along six corners of a hexagon, which is defined by the in-plane triaxial MCA of the (111)-grown YIG sample [22]. We note that the reorientation pattern is different for the horizontal and nearly vertical initial states, with the horizontal case showing clearer reorientation along the other two easy axes [Fig. 4(c)] compared to the reorientation induced when the magnetization is initially oriented off axis [Fig. 4(f)].

We find that the micromagnetic simulations broadly explain the experimentally observed features. In Figs. 3(a)–3(d), the magnetization undergoes reorientation on an ultrafast timescale, forming four distinct domains that are stabilized by the different axes of in-plane MCA. We stress that in the magneto-optical images of Fig. 2, we are only sensitive to the out-of-plane component of the magnetization, with the in-plane component inferred from the direction of the stripes. In the simulation results shown in Fig. 3, in contrast, we resolve the in-plane component of magnetization. The reorientation of the in-plane magnetization vector, in the simulations, therefore corresponds with the observed reorientation of the stripe domains in the experiment. Keeping this fact in mind, our

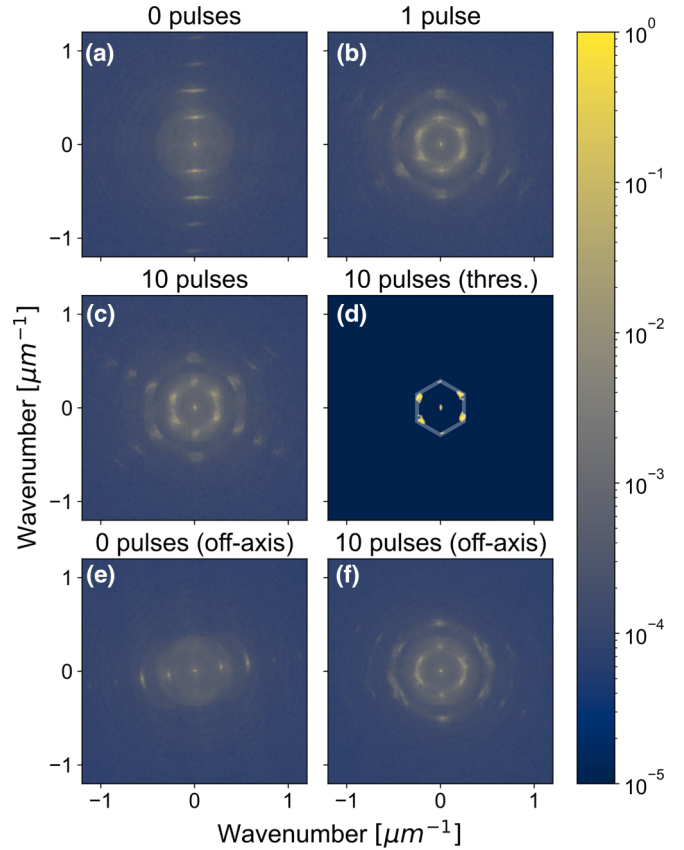


FIG. 4. (a)–(c) Normalized two-dimensional Fourier transforms of the magneto-optical images taken after exposing the YIG sample to the indicated number of IR pulses. The magnetic stripe domains were initially oriented horizontally. (d) Same as (c) but thresholded (threshold value 10^{-2}) with a hexagon overlaid with a circumscribed radius of $0.288 \mu\text{m}^{-1}$. (e), (f) Normalized two-dimensional Fourier transforms of the magneto-optical images taken after exposing the YIG sample to the indicated number of IR pulses. The magnetic stripe domains were initially oriented close to the vertical axis.

micromagnetic simulations qualitatively correlate with the experimental measurements, through the reorientation along the different anisotropy axes [Figs. 2(b) and 2(c)], although the experimental results show much more disordered magnetic domains. This can be explained by the fact that we experimentally irradiate the sample with approximately 200 pulses rather than 1, which introduces fluctuations of the pulse energy and therefore slight fluctuations in the affected area.

The micromagnetic simulations also allow us to understand the driving force behind the observed reorientation of magnetic domains, and its spatial footprint. The incident spatially Gaussian pulse induces displacement in the YIG sample that is presumably similarly Gaussian in profile. Further, the radial symmetry of this spatial distribution of displacement generates uniaxial MCA with radial symmetry [13,33]. In combination with the initial distribution of magnetization, the elastic strain is used to calculate the magnetoelastic energy density [Eq. (1)] and the magnetoelastic field B_{mel} [Fig. 3(f)]. The latter exerts torque on the magnetization, which is maximum in the four quadrants about the center. This explains both the observed twofold rotational symmetry of the reorientation

pattern and why the distribution of reoriented magnetization is extended along the x axis.

Noticeably, the domains of reoriented magnetization were observed (in both the experiments and micromagnetic simulations) to grow substantially in size with the application of additional pulses [Fig. 2(d)], which is in stark contrast to the results shown in Ref. [13]. This behavior can be understood by inspecting Figs. 3(e) and 3(f). After the application of several pulses, the magnetization relaxes to form the reoriented distribution shown in Fig. 3(e), with the magnetization stabilized by the in-plane triaxial MCA. The subsequent application of the pulse generates the same B_{mel} field as shown in Fig. 3(f). The latter is still noncollinear with the magnetization, thus allowing it to exert nonzero torque and thereby further reorient the magnetization.

In conclusion, we have shown that the stripe magnetic domains characteristic of YIG in its ground state can be reori-

ented by IR pulses. The reorientation is spatially nonuniform, and can be understood as a consequence of the nonuniform strain that is applied by the pulse. As an outlook, a more complete understanding of the microscopic mechanism underpinning the reorientation must be developed. In order to achieve this goal, the magnetization dynamics governing the interaction of the IR pulse, the subsequent strain wave, and the magnetic system should be studied with temporal resolution approaching picosecond timescales.

Acknowledgments. We acknowledge the Nederlandse Organisatie voor Wetenschappelijk Onderzoek (NWO-I) for their financial contribution, including the support of the FELIX Laboratory, and also acknowledge the networking opportunities provided by the European COST Action CA17123 “Magnetofon.” We thank S. O. Demokritov for providing the YIG sample and for fruitful discussions, and all technical staff at FELIX for providing technical support.

-
- [1] L. D. Stevens, The evolution of magnetic storage, *IBM J. Res. Dev.* **25**, 663 (1981).
- [2] A. V. Kimel and M. Li, Writing magnetic memory with ultrashort light pulses, *Nat. Rev. Mater.* **4**, 189 (2019).
- [3] M. A. Khan, J. Sun, B. Li, A. Przybysz, and J. Kosel, Magnetic sensors—A review and recent technologies, *Eng. Res. Express* **3**, 022005 (2021).
- [4] P. C. Lauterbur, Image formation by induced local interactions: Examples employing nuclear magnetic resonance, *Nature (London)* **242**, 190 (1973).
- [5] D. A. Alromi, S. Y. Madani, and A. Seifalian, Emerging application of magnetic nanoparticles for diagnosis and treatment of cancer, *Polymers* **13**, 4146 (2021).
- [6] R. E. Rottmayer, S. Batra, D. Buechel, W. A. Challener, J. Hohlfeld, Y. Kubota, L. Li, B. Lu, C. Mihalcea, K. Mountfield, K. Pelhos, C. Peng, T. Rausch, M. A. Seigler, D. Weller, and X.-M. Yang, Heat-assisted magnetic recording, *IEEE Trans. Magn.* **42**, 2417 (2006).
- [7] A. Stupakiewicz, K. Szerenos, D. Afanasiev, A. Kirilyuk, and A. V. Kimel, Ultrafast nonthermal photo-magnetic recording in a transparent medium, *Nature (London)* **542**, 71 (2017).
- [8] C. D. Stanciu, F. Hansteen, A. V. Kimel, A. Kirilyuk, A. Tsukamoto, A. Itoh, and T. Rasing, All-optical magnetic recording with circularly polarized light, *Phys. Rev. Lett.* **99**, 047601 (2007).
- [9] I. Radu, K. Vahaplar, C. Stamm, T. Kachel, N. Pontius, H. A. Dürr, T. A. Ostler, J. Barker, R. F. L. Evans, R. W. Chantrell, A. Tsukamoto, A. Itoh, A. Kirilyuk, T. Rasing, and A. V. Kimel, Transient ferromagnetic-like state mediating ultrafast reversal of antiferromagnetically coupled spins, *Nature (London)* **472**, 205 (2011).
- [10] T. A. Ostler, J. Barker, R. F. L. Evans, R. W. Chantrell, U. Atxitia, O. Chubykalo-Fesenko, S. E. Moussaoui, L. L. Guyader, E. Mengotti, L. J. Heyderman, F. Nolting, A. Tsukamoto, A. Itoh, D. Afanasiev, B. Ivanov, A. M. Kalashnikova, K. Vahaplar, J. Mentink, A. Kirilyuk, Th. Rasing *et al.*, Ultrafast heating as a sufficient stimulus for magnetization reversal in a ferrimagnet, *Nat. Commun.* **3**, 666 (2012).
- [11] C. S. Davies, T. Janssen, J. H. Mentink, A. Tsukamoto, A. V. Kimel, A. F. G. van der Meer, A. Stupakiewicz, and A. Kirilyuk, Pathways for single-shot all-optical switching of magnetization in ferrimagnets, *Phys. Rev. Appl.* **13**, 024064 (2020).
- [12] C. H. Lambert, S. Mangin, B. S. D. C. S. Varaprasad, Y. K. Takahashi, M. Hehn, M. Cinchetti, G. Malinowski, K. Hono, Y. Fainman, M. Aeschlimann, and E. E. Fullerton, All-optical control of ferromagnetic thin films and nanostructures, *Science* **345**, 1337 (2014).
- [13] A. Stupakiewicz, C. S. Davies, K. Szerenos, D. Afanasiev, K. S. Rabinovich, A. V. Boris, A. Caviglia, A. V. Kimel, and A. Kirilyuk, Ultrafast phononic switching of magnetization, *Nat. Phys.* **17**, 489 (2021).
- [14] P. Stremoukhov, C. S. Davies, A. Safin, S. Nikitov, and A. Kirilyuk, Phononic manipulation of antiferromagnetic domains in NiO, *New J. Phys.* **24**, 023009 (2022).
- [15] T. Janssen, M. Gidding, C. S. Davies, A. V. Kimel, and A. Kirilyuk, Strain-induced magnetic pattern formation in antiferromagnetic iron borate, *Phys. Rev. B* **108**, L140405 (2023).
- [16] M. Kwaaitaal, D. G. Lourens, C. S. Davies, and A. Kirilyuk, Epsilon-near-zero regime as the key to ultrafast control of functional properties of solids, *arXiv:2305.11714*.
- [17] A. Subedi, A. Cavalleri, and A. Georges, Theory of nonlinear phononics for coherent light control of solids, *Phys. Rev. B* **89**, 220301(R) (2014).
- [18] G. Khalsa, and J. Z. Kaaret, and N. A. Benedek, Coherent control of the translational and point group symmetries of crystals with light, *Phys. Rev. B* **109**, 024110 (2024).
- [19] M. Gidding, T. Janssen, C. S. Davies, and A. Kirilyuk, Dynamic self-organisation and pattern formation by magnon-polarons, *Nat. Commun.* **14**, 2208 (2023).
- [20] J. M. Robertson, Liquid phase epitaxy of garnets, *J. Cryst. Growth* **45**, 233 (1978).
- [21] A. Hubert and R. Schäfer, *Magnetic Domains: The Analysis of Magnetic Microstructures* (Springer, Berlin, 2009).
- [22] M. Wu, *Nonlinear Spin Waves in Magnetic Film Feedback Rings* (Academic Press, New York, 2010), pp. 163–224.
- [23] D. Oepts, A. F. G. van der Meer, and P. van Amersfoort, The free-electron-laser user facility FELIX, *Infrared Phys. Technol.* **36**, 297 (1995).
- [24] See Supplemental Material at <http://link.aps.org/supplemental/10.1103/PhysRevB.109.L060408> for additional information on the FELIX pulse structure, the derivation of the strain tensor

- used to model the pump pulse, and the source images used to calculate the Fourier transforms of Fig. 4, which includes Ref. [13].
- [25] A. Vansteenkiste, J. Leliaert, M. Dvornik, M. Helsen, F. Garcia-Sanchez, and B. Van Waeyenberge, The design and verification of MuMax3, *AIP Adv.* **4**, 107133 (2014).
- [26] S. Klingler, A. V. Chumak, T. Mewes, B. Khodadadi, C. Mewes, C. Dubs, O. Surzhenko, B. Hillebrands, and A. Conca, Measurements of the exchange stiffness of YIG films using broadband ferromagnetic resonance techniques, *J. Phys. D: Appl. Phys.* **48**, 015001 (2015).
- [27] D. Stancil and A. Prabhakar, *Spin Waves: Theory and Applications* (Springer, New York, 2009).
- [28] V. H. Ortiz, B. Arkook, J. Li, M. Aldosary, M. Biggerstaff, W. Yuan, C. Warren, Y. Kodera, J. E. Garay, I. Barsukov, and J. Shi, First- and second-order magnetic anisotropy and damping of europium iron garnet under high strain, *Phys. Rev. Mater.* **5**, 124414 (2021).
- [29] E. R. Rosenberg, L. C. V. Beran, C. O. Avci, C. Zeledon, B. Song, C. Gonzalez-Fuentes, J. Mendil, P. Gambardella, M. Veis, C. Garcia, G. S. D. Beach, and C. A. Ross, Magnetism and spin transport in rare-earth-rich epitaxial terbium and europium iron garnet films, *Phys. Rev. Mater.* **2**, 094405 (2018).
- [30] A. A. Serga, A. V. Chumak, and B. Hillebrands, YIG magnonics, *J. Phys. D: Appl. Phys.* **43**, 264002 (2010).
- [31] A. G. Gurevich and G. A. Melkov, *Magnetization Oscillations and Waves* (CRC Press, Boca Raton, FL, 1996).
- [32] A. B. Smith and R. V. Jones, Magnetostriction constants from ferromagnetic resonance, *J. Appl. Phys.* **34**, 1283 (1963).
- [33] A. W. Rushforth, E. De Ranieri, J. Zemen, J. Wunderlich, K. W. Edmonds, C. S. King, E. Ahmad, R. P. Campion, C. T. Foxon, B. L. Gallagher, K. Vyborny, J. Kučera, and T. Jungwirth, Voltage control of magnetocrystalline anisotropy in ferromagnetic-semiconductor-piezoelectric hybrid structures, *Phys. Rev. B* **78**, 085314 (2008).